Exploring the entrance of proton pathways in cytochrome *c* oxidase from *Paracoccus denitrificans:* Local buffer capacity and redox-dependent polarity changes at the internal surface

Kristina Kirchberg[1,2], Hartmut Michel[2*], and Ulrike Alexiev[1*]

From Physics Department[1], Freie Universität Berlin, Berlin, Germany and

Department of Molecular Membrane Biology[2], Max-Planck-Institute of Biophysics, Frankfurt a.M., Germany

*Address correspondence to: Ulrike Alexiev, Department of Physics, Freie Universität Berlin, Arnimallee 14, D-14195 Berlin, Germany, Phone: +49-30-838-55157; Fax: +49-30-83856510; E-mail: alexiev@physik.fu-berlin.de

Hartmut Michel, Department of Molecular Membrane Biology, Max Planck Institute of Biophysics, Max-von-Laue Str. 3, D-60438 Frankfurt/Main, Germany, Phone: +49-69-6303-1001; Fax: +49-69-6303-1002; E-mail: Hartmut.Michel@biophys.mpg.de

Abstract

Cytochrome *c* oxidase (C*c*O), the terminal oxidase of cellular respiration, reduces molecular oxygen to water. The mechanism of proton pumping as well as the coupling of proton and electron transfer is still not understood in this redox-linked proton pump. Eleven residues at the aqueous-exposed surfaces of C*c*O from *Paracoccus denitrificans* have been exchanged to cysteines in a two-subunit base variant to yield single reactive cysteine variants. These variants are designed to provide unique labeling sites for probes to be used in spectroscopic experiments investigating the mechanism of proton pumping in C*c*O.

To this end we have shown that all cysteine variants are enzymatically active. Cysteine positions at the negative (N-) side of the membrane are located close to the entrance of the D- and K-proton transfer pathways that connect the N-side with the catalytic oxygen reduction site. Labeling of the pH-indicator dye fluorescein to these sites allowed us to determine the surface potential at the cytoplasmic C*c*O surface, which corresponds to a surface charge density of -0.5 elementary charge/1000 $Å^2$. In addition, acid–base titrations revealed site-specific values of buffer capacity at the surface. Polarity measurements of the label environment at the N-side provided (i) site-specific values indicative of a hydrophilic and a more hydrophobic environment dependent on the label position, and (ii) information on a global change to a more apolar environment upon reduction of the enzyme. Thus, the redox state of the copper and heme centers inside the hydrophobic interior of C*c*O affect the properties at the cytoplasmic surface.

Keywords: Cytochrome *c* oxidase, pH-indicator dye, covalent surface labeling, surface potential, buffer capacity, fluorescein

Abbreviations:

C*c*O: Cytochrome c oxidase, IAF: 5-Iodoacetamidofluorescein, LM: *n*-Dodecyl-β-D-maltoside, LDAO: Lauryldimethylamine-oxide, CS: cysteine-less base variant, Flu: Fluorescein sodium salt

1. Introduction

Cytochrome *c* oxidase (C*c*O), the terminal enzyme of the respiratory chain of mitochondria and many aerobic prokaryotes, catalyzes the reduction of molecular oxygen to water. This redox reaction, consuming four "substrate" protons, is coupled to the translocation of additional four "pumped" protons across the membrane to further increase the electrochemical proton gradient, which is the driving force for ATP synthesis by the ATP-synthase. Two separate proton pathways have been suggested for the bacterial C*c*O, leading from the N- (negative) side (cytoplasmic side) of the membrane towards the heme-copper site (Fig. 1): the so-called D- and K-pathways [1-5]. The K-pathway, named after the conserved amino acid K354 (*Paracoccus denitrificans* C*c*O amino acid numbering), is located close to the protein/lipid interface (Fig. 2C) and leads straight to the active site. This pathway may be involved in the delivery of the first one or two protons during the reduction of the oxidized enzyme. The D-pathway starts at D124 directly at the cytoplasmic surface of CcO (Fig. 2B) and leads to another highly conserved residues, E278 (Fig. 1). It appears to be the only pathway required when the fully reduced C*c*O reacts with molecular oxygen [6-9]. Since the D-pathway is likely to be involved in the uptake of all "pumped" protons as well as of two or three of the "substrate" protons, E278 is considered to be the branching point beyond which a proton is either transported to the binuclear center for O_2 reduction to water or translocated (proton pumping) to the opposite side of the membrane via an yet unidentified route. In this route, a proton loading (or pump) site is postulated [10], which alternates proton affinity depending on the redox state of the active site and serves as an acceptor for protons waiting to be pumped [11]. The pumping itself appears to be caused by electrostatic repulsion from another proton which enters the binuclear site and is consumed there in the chemical reaction, in accordance with the "principle of electroneutrality" [12]. A protein conformational change, however, could also be responsible for the coupling and is the subject of controversy [13-15]. Small conformational changes between oxidized and reduced crystal structures have been reported for bovine oxidase (for a review see [16]) and recently also for the bacterial oxidase from *Rhodobacter sphaeroides* [13]. The latter result suggests a conformational control of alternate opening of the D- and K-pathways that fits with the hypothesis that the K-pathway is closed in the oxidative phase [17]. Little is known about the exit pathway to the P- (positive) side of the membrane where multiple exit routes appear to exist [4].

The assignment of proton uptake and proton pumping to the individual steps of the catalytic cycle of C*c*O is still a matter of debate [6, 18-28]. Proton uptake and release kinetics using soluble pH indicator dyes and time-resolved absorption spectroscopy were measured in the different steps of the catalytic cycle. Photo-injection of single electrons into different intermediate states [18, 29] or flow-flash measurements to trigger the reaction of fully reduced C*c*O with O_2 were employed [15, 30-33]. The latter type of experiments revealed a high sensitivity to kinetic isotope effects in those steps that are associated with proton transfer to the internal proton acceptor (pump) site [15], suggesting the

involvement of a conformational change. A similarity to the proton pump bacteriorhodopsin was noted [28], where large kinetic isotope effects exist in the L→M transition [34] which involves proton transfer from the retinal Schiff base to the internal proton acceptor D85. Also in bacteriorhodopsin, transient deprotonation of the internal proton donor and proton uptake were found to be connected to conformational and surface potential changes at the cytoplasmic surface [34-37].

In a recent study about proton transfer reactions in the O→E transition of *P. denitrificans* C*c*O we reported that both H^+-uptake and release steps during single-electron injection into oxidized C*c*O precede net H^+-uptake [18]. Initial H^+-uptake coincides with electron input into Cu_A at the opposite membrane side. This suggests efficient H^+-uptake mechanisms, such as proton collecting antennae [38, 39] switched on by electron injection [18]. Proton-collecting antennae are negative surface patches to concentrate protons at the membrane surface and to funnel these protons into the orifice of a proton pathway. They appear to consist of several carboxylates (glutamic or aspartic acids) within hydrogen-bonded networks, histidine residues as buffering molecules and threonines as microswitches (Fig. 2 B, C) [38-40].

To further understand the mechanism of proton pumping, as well as the involvement of proton collecting antennae and conformational changes in bacterial C*c*O we have constructed single reactive cysteine C*c*O variants to explore the C*c*O surface and the entrance of the proton pathways. These cysteine residues provide selective binding sites for various reporter molecules, such as fluorescence labels for conformational changes, pH indicator dyes for protonation reactions, or polarity probes for sensing the local environment [35, 36, 41-44]. We have constructed eleven single cysteine C*c*O variants. Three positions at the P-side, and eight positions at the N-side, close to the entrance of the D- and K-pathways, were exchanged to cysteine. All cysteine variants exhibit wild-type like oxidase activity. The different positions at the surface were tested for labeling with the pH-sensitive dye fluorescein. Spectroscopic characterization revealed a distinct polarity and surface buffering capacity pattern at the entrance of both the D– and K–proton pathways. Polarity changes upon reduction of the enzyme were observed, indicating different surface properties in the oxidized and reduced forms of C*c*O. This observed change suggests a redox-linked control of surface properties at the N-side of C*c*O, presumably mediated by subtle conformational changes.

2. Materials and Methods

2.1 Materials

n-Dodecyl-β-D-maltoside was from GLYCON Biochemicals GmbH (Luckenwalde, Germany). 5-iodoacetamidofluorescein was from Invitrogen/Molecular probes. All other chemicals were of the highest grade available. The expression vector pKH160 and the strain ORI14 were grateful gifts from K. Hoffmeier and O. Richter from Prof. B. Ludwig's group, Frankfurt a. M., Germany.

*2.2 Construction of cysteine C*c*O variants*

Amino acids to be exchanged to cysteine were selected for mutagenesis on the basis of the crystal structure of the *Paracoccus* cytochrome *c* oxidase [3, 45]. Site-directed mutagenesis was performed according to the "quickchange" protocol of Stratagene (Heidelberg, Germany). All mutations introduced into the ctaDII gene encoding subunit I and the ctaC gene encoding subunit II were confirmed by DNA sequencing.

To perform site-directed mutagenesis in subunits I and II of *P. denitrificans* C*c*O the XbaI-NdeI-fragment containing the ctaDII- and the ctaC-gene of the expression vector pKH160 containing genes for subunit I, II and III was subcloned into the XbaI-NdeI-cleaved pUC18 vector [46] yielding the vector pKK1 with a reduced plasmid size of ~ 5k base pairs compared to ~ 13k base pairs of pKH160. In a first the step, a quasi cysteine-less base variant (CS) of subunits I and II was constructed. Surface exposed cysteines in position 44, and 140 in subunit I were mutated into serines. Essential cysteines, such as C216 and C220 which serve as ligands for Cu_A, and the pair C66/C80 which forms a disulfide bridge as well as cysteines in the protein core (in position 50 and 56 of subunit II) were not changed. In a second step, amino acids in eleven different positions were replaced by cysteines within the plasmid pKK1-CS to yield CS-T26C, CS-N27C, CS-P123C, CS-P128C, CS-S295C, CS-K299C, CS-P301C, CS-P302C in subunit I, and CS-H^{II}29C, CS-D^{II}30C, and CS-R^{II}130C in subunit II. After the successful exchange of the desired base pairs, the respective XbaI-NdeI-fragment was cloned back into the cleaved expression vector pKH160.

*2.3 Expression and purification of C*c*O.*

The expression vector pKH160 with the XbaI-NdeI-fragment containing the respective cysteine mutations was conjugated into the *Paracoccus* recipient strain ORI14 (MR31-derivative, ΔctaDI::Kmr ΔctaDII::Tetr Δcta-operon::Gmr), lacking the genes for subunit I, II and III. Cells were grown on succinate medium [47], supplemented with 25µg/ml streptomycin sulfate and 25 µg/ml kanamycin at 32°C. Enzyme preparation of core subunits I and II and variants was performed as described [48], followed by the addition of 0.1% LDAO to detach the core subunits from subunit III and IV. Separation and detergent exchange was done on a Q-Sepharose FF ion exchange column.

For complete reduction of C*c*O 2 mM sodium dithionite was added to the solution.

2.4 Spectroscopic methods

UV/Vis absorption spectra were recorded with a Shimadzu UV2450 spectrophotometer.

2.5 Determination of enzymatic activities of isolated CcO.

Cytochrome *c* oxidase activity was determined as described previously [49]. Reduced horse heart cytochrome *c* was used at a concentration of 50 µM in 10 mM potassium phosphate buffer pH 7.4, 40 mM KCl, 1 mM EDTA and 0.05 % LM at room temperature. The rate of cytochrome *c* oxidation was measured by following the change in absorbance at 550 nm.

2.6 Labeling with 5-iodoacteamidofluorescein

For the labeling of C*c*O with IAF to a solution of 50 µM C*c*O in 10 mM potassium phosphate buffer pH 7.5, 50 mM KCl and 0.05% LM a tenfold molar excess of 5-IAF over C*c*O was added. The mixture was allowed to react for 1h at room temperature in the dark. Unbound label was removed via gel filtration. The labeling stoichiometry was calculated spectroscopically from the absorbance at 425 nm of C*c*O and the absorbance change of fluorescein at 495nm:

$$\frac{[F]}{[CcO]} = \frac{\Delta A_{495}}{\Delta A_{425}} \frac{\varepsilon_{425}(CcO)}{\Delta\varepsilon_{495}(F)} \qquad (1)$$

with

$$\Delta A_{495} = \Delta A_{495}(pH9.5) - \Delta A_{495}(pH5.5) \qquad (2)$$

The extinction coefficients are $\Delta\varepsilon_{495\ nm}$ = 36 000 M^{-1} cm^{-1} (calculated from the value for the alkaline form of fluorescein given by Molecular Probes) and $\varepsilon_{425\ nm}$ = 158 mM^{-1} cm^{-1} for C*c*O. Covalent labeling was checked via SDS polyacrylamide gel electrophoresis.

2.7 Determination of buffer capacity at the enzyme surface

To identify the buffer capacity of CcO at a given pH value, the absorbance changes of the CcO-bound pH indicator dye fluorescein in response to a small perturbation of the titrant (acid/base) was determined. In this way, absorbance changes of fluorescein relate to pH changes that will depend on the buffer capacity at the pH value concerned. The changes in absorbance ΔA were followed at 495 nm (fluorescein) and normalized to the changes in proton concentration Δc_{H+} yielding $\Delta A/\Delta c_{H+}$. This ratio is inverse proportional to the buffer capacity. The higher the amount of buffer molecules (fixed or mobile) the smaller is the $\Delta A/\Delta c_{H+}$ value. The absorbance of fluorescein was titrated in a solution containing 5 µM C*c*O with a defined small amount of 10 mM potassium hydroxide and hydrochloric acid in alternating steps at a given pH value (pH 7.3).

2.8 Determination of surface charge density

The salt dependence of the apparent pK_a of the covalently bound pH indicator dye was used to determine the surface charge density. Fluorescein-labeled C*c*O was titrated in different salt concentrations and the spectra were recorded. Analysis of titration experiments was performed as described [50]. To obtain the apparent pK_a, the measured absorbance changes ΔA of fluorescein at 495 nm were fitted with the Henderson-Hasselbalch equation:

$$\Delta A = \frac{\Delta A_{\max}}{1+10^{n(pK-pH)}} \tag{3}$$

with ΔA_{max} the maximum of the difference in absorbance between the alkaline (dianionic) and the monoanionic form of fluorescein, *n* the number of protons involved in the transition, and p*K* the midpoint of the titration curve. From the difference between the apparent pK_a (pK_{app}) at a given salt concentration and the intrinsic (true) pK_a (pK_t), the surface potential φ can be determined using the Boltzmann equation:

$$pK_t - pK_{app} = e\varphi / 2.3kT \tag{4}$$

The surface charge density σ is then calculated from the surface potential φ using the Gouy-Chapman equation:

$$\sigma = \frac{c^{1/2}}{B}\sinh\left(\frac{e\varphi_0}{2kT}\right) \tag{5}$$

c is the salt concentration of the symmetric, monovalent electrolyte (KCl). B [$B = (8\varepsilon\varepsilon_0 N_A kT)^{-1/2}$] equals 134.6 $M^{1/2}$ assuming a dielectric constant ε of 78.5 at 22°C, ε_0 is the permittivity of free space, N_A is the Avogadro constant and *k* is the Boltzmann constant. The pK_t was calculated by extrapolation of pK_{app} to infinite salt concentration with a transformed Gouy-Chapman equation [51]:

$$10^{pK_{app}} = (-2B\sigma 10^{pK_t/2})10^{pK_{app}/2}C^{-1/2} + 10^{pK_t} \tag{6}$$

From Eq. (6), the surface charge density σ and the true pK_t can be determined from the slope and the intercept of the ordinate, respectively.

3. Results

*3.1 Biochemical and spectroscopic characterization of cysteine C*c*O variants.*

Eleven single reactive cysteine C*c*O variants in the CS background were prepared. Residues at three positions at the P-side (in subunit II: H29, D30, R130), and at eight positions at the N-side (T25, N27, P123, P128, S293, K299, P301, I302), close to the entrance of the D- and K-pathways, were replaced by cysteines (Fig. 2). The single reactive cysteine variants have absorption spectra which are very similar to those of wild type (Fig. 3). A comparison of absorption spectra from oxidized (red) and reduced (cyan) samples of the CS variant and wild-type C*c*O (black dotted lines) is presented in Fig. 3 showing virtually identical spectra. The kinetics of cytochrome *c* oxidation after addition of the respective cysteine C*c*O variant was measured by following the change in absorbance at 550 nm (Fig. 3 CS inset). The respective turnover numbers were calculated and found to be similar to wild type (Tab.1).

*3.2 Attachment of fluorescein to cysteine residues in C*c*O.*

The purified C*c*O cysteine variants were modified with fluorescein (IAF) according to the reaction conditions described in *Materials and Methods* yielding samples with fluorescein covalently bound to the single reactive cysteine residue (C-AF). In the CS base variant no incorporation of fluorescein was detected under these conditions (Tab. 2, Fig. 4B lane 3). Figure 4A shows the absorption spectra of labeled and unlabeled CS-I302. Position 302 is located in subunit I in close vicinity to the entrance of the K-pathway. The absorption band of fluorescein is marked with an arrow. Covalent binding of fluorescein was verified by the fluorescence of the subunit I band following SDS-PAGE (Fig. 4B). The incorporation of fluorescein varied with the labeling position and the labeling stoichiometries are listed in Table 2. C*c*O variants with cysteines at the P-side could not be labeled with fluorescein under the reported labeling conditions, presumably due to the lack of accessibility of their sulfhydryl groups to the bulky fluorescein or unfavorable local surface pH conditions. At the N-side labeling stoichiometries between 0.25 and 0.92 mol AF per mol C*c*O were achieved, except for position 27. Labeling with fluorescein did not affect function as shown by the absorption spectra of oxidized and reduces samples (Fig. 4C) that resemble those of wild type (Fig. 3).

3.3 Surface charge density at the N-side

Fluorescein has a pH-sensitive absorption spectrum with the maximum at ~490 nm in the alkaline form. A typical set of absorption spectra at various pH values and the absorption spectra of CS-I302C-AF at pH 9 is shown in Figure 5 A and B, respectively. In addition to the dye absorbance changes, a transition may occur in the C*c*O absorption. As a control, the pH dependent spectra of CS-I302C not labeled with fluorescein are presented in Figure 5C. These spectra are characterized by minor changes in absorbance around 470 nm and 540 nm and an isosbestic point at 496 nm. Compared

to the absorbance changes of fluorescein around 500 nm, the absorbance differences due to C*c*O in this wavelength region are negligible.

When fluorescein was bound to C*c*O, its pK_{app} in 150 mM KCl was 7.1, clearly higher than the pK_a of 6.3 determined for unbound IAF [50]. Moreover, the pK_{app} of bound fluorescein was highly salt dependent. Figure 6A demonstrates, as an example, pH titration curves for CS-I302C-AF at various salt concentrations. The pK_{app} decreased with increasing salt concentration from pK_{app} = 7.54±0.06 at 10 mM KCl to 7.11±0.07 at 0.15 M KCl. For all titration curves the number of protons involved in the transition was n = 1±0.05, indicating that in the pH range from 6.5 to 9 the protonation/deprotonation reaction of the dye is not affected by the deprotonation of other groups in the C*c*O-micelle. The surface charge density appears to be constant in this pH range. The salt dependence of the apparent pK was used to calculate the surface charge density according to the equations described under *Materials and Methods* (Fig. 6). The charge density on the cytoplasmic side, determined in position 302 is 0.5 e^- /1000 A^2. According to X-ray structural models [4] this residue is located directly at the surface (Fig. 2) and the surface charge density can be regarded as a representative value. The true pK of fluorescein bound at position 302, i.e the pK in the absence of surface potential at infinitive high salt concentrations, was determined with pK_t =7.0 (Fig. 6B).

3.4 Local buffer capacity

Protonable groups at protein and membrane surfaces can act as immobile buffer molecules [52]. They contribute to the local buffer capacity at the protein surface. Under equilibrium conditions the absorbance change of the bound pH indicator dye fluorescein in response to defined changes in proton concentration in the absence of any mobile buffer molecules yields a normalized dye protonation value $\Delta A/\Delta c_{H+}$ for evaluating the buffer capacity of the enzyme. The smaller the $\Delta A/\Delta c_{H+}$ value the higher is the buffer capacity. The $\Delta A/\Delta c_{H+}$ values for fluorescein attachment sites in the vicinity of the D- and K-pathway entrance are summarized in Table 3. The values are similar within the given errors and yield a mean value of 0.2± 0.1 mOD/µM in the oxidized state of the enzyme. From the similarity of the $\Delta A/\Delta c_{H+}$ values at the various sites we conclude that all enzyme-bound fluoresceins are accessible for proton binding. Since the values were determined in C*c*O micelles, the contribution of detergent and protein surface was tested by adding soluble fluorescein to C*c*O micelles and empty detergent micelles. We found a higher buffer capacity in the presence of *CcO* compared to the situation when only detergent micelles are present (Tab. 3). The data indicate that the high buffer capacity results from the fixed buffer molecules at the enzyme surface. The $\Delta A/\Delta c_{H+}$ values found here for C*c*O (1.1 mOD/µM) are smaller than those measured for bacteriorhodopsin-CHAPS micelles (U. Alexiev, unpublished results), i.e. the buffer capacity is higher for CcO, and were reproduced in bacteriorhodopsin-LM micelles with 3.7 mOD/µM (Tab. 3).

*3.5 Polarity of label environment and polarity changes upon C*c*O reduction*

A shift of the λ_{max} of fluorescein absorption from 490 nm in the unbound form to 502 nm upon binding to cysteine in position 302 is clearly visible in Figure 5, indicating an environmental effect. The absorption maximum of fluorescein is dependent on the polarity of the solvent and shifts to higher wavelength when the solvent becomes more apolar [43] (Fig. 7C). A dependence of the dye absorption maximum on the label position could thus provide information on the polarity of its environment.

In Figure 7 D and E the absorption maxima of fluorescein determined in the different label positions at the N-side of oxidized C*c*O are summarized. A dependence of the absorption maximum on the label position is apparent. Roughly two classes of fluorescein positions could be distinguished. At the entrance of the D-pathway (Fig. 7D) the dye at position 26, 123 and 128 exhibits λ_{max}-values between 497 and 498 nm, indicative of an orientation of the label towards a more hydrophilic environment, compared to the 502 nm value found in position 302. Variations in λ_{max}–values were found at the entrance of the K-pathway (Fig. 7E). The λ_{max}–values are 501-502.5 nm for fluorescein in position 295, 299, and 302, while a value of 497 nm was obtained in position 301.

To determine the λ_{max} of fluorescein absorption in the reduced state of the enzyme, we also have to take the transition in CcO absorption into account that may occur at the wavelengths of the fluorescein absorption band. As a control, the difference spectrum of oxidized and reduced CcO is shown in Fig. 7 A. At about 500 nm only marginal changes in absorbance are visible (arrow in Fig. 7A), in comparison to the large absorbance values of the fluorescein (Fig. 4 A,C). Using CS-T26C-AF as an example, we show the fluorescein difference spectra by subtracting the spectrum of the respective unlabeled sample in Figure 7B. A clear shift of the absorption maximum of bound fluorescein to longer wavelengths upon reduction of the enzyme is visible. The positive shift of the λ_{max}–values seems to be independent of the labeling position (Fig. 7 D,E). The data indicate a global change at the N-side of C*c*O, which probably results in a more apolar environment at the protein surface.

4. Discussion

Cysteine variants, in particular of membrane proteins, have been used widely as labeling sites for various reporter groups to investigate surface conformation, surface protonation, surface potential or polarity of the local environment (e.g. [35, 36, 41, 43, 44]). Here, we designed 11 cysteine variants to be used as labeling sites to explore the entrance of the D- and K-pathway at the N-side of C*c*O as well as the region of proton exit at the P-side of the membrane. At the N-side we have selected the positions to be exchanged for cysteine such that they are located around the orifice of the D- and K-pathway. Care was taken not to interfere with a putative proton collecting antenna, no carboxylate or histidine was exchanged at this side. All cysteine variants exhibit wild-type-like behavior. Labeling with the pH indicator dye fluorescein also did not affect the integrity of the enzyme as judged from the absorption spectra of the oxidized and reduced forms of the enzyme.

The pH indicator dye fluorescein can be used amongst others to characterize proton release and uptake kinetics at the surface of a proton pump [41, 43, 44], surface potential and surface potential changes [36, 50], protein conformational changes or apparent protonation exchange rates of a single fluorescein attached to the surface [53]. In this report we used the attached fluorescein to investigate the surface charge density, local buffer capacity and polarity of the environment at the cytoplasmic side of C*c*O.

We determined the surface charge density directly at the desired membrane surface, based on the dependence of the apparent pK_a of a surface-bound pH indicator dye on the salt concentration. The validity of this method was tested in detail with bacteriorhodopsin [36]. In accordance with the localisation of position 302 at the cytoplasmic surface of C*c*O micelles, i.e. the N-side of the membrane, a negative surface charge density was determined for the protein surface that contributes to the negative potential at this side of the membrane.

The buffer capacity measured here for the redox-linked proton pump CcO is much higher than for the proton pump bacteriorhodopsin. Since in our measurements the buffer capacity originates from fixed buffer sites at the protein, we have to compare the amino acid composition at the surface of C*c*O and bacteriorhodopsin. It is evident that in contrast to C*c*O the aqueous exposed surfaces of bacteriorhodopsin do not contain histidines. Histidines are supposed to play an important role as buffer residues in the proposed proton collecting antennae [54]. Three histidines were found close to the entrance of the D-pathway (Fig. 2B), one histidine close to the entrance of the K-pathway, and several more distributed across the cytoplasmic surface of C*c*O (Fig. 2C). It is therefore not surprising that the buffer capacity of C*c*O exceeds the values found for bacteriorhodopsin (Tab. 3).

Furthermore, the different absorption maxima of the attached fluorescein indicate different environments for the orientation of the label. For fluorescein bound to bacteriorhodopsin in the DE-loop a clear dependence on the orientation of the label was observed in an earlier report [43]. The absorption maximum of fluorescein oriented towards the detergent shell was at 502 nm, while the λ_{max} values of fluorescein oriented towards the proton channel were at ~498 nm. Using these values as

reference, fluorescein in position 26, 123 and 128 at the entrance of the D-pathway is in contact with a hydrophilic environment. At the entrance of the K-pathway fluorescein bound to position 301 is in contact with a hydrophilic environment, while the dye in position 295, 299, and 302 experiences a more hydrophobic environment. Information about localization of the bound pH indicator dye is important for future experiments on protonation rates in these sites. Independent of the labeling site we found a shift in the dye absorption spectrum upon reduction of the enzyme, indicating that the whole cytoplasmic surface becomes more apolar. The data point to a global change that is related to the redox state of the enzyme, however, the molecular basis of this effect is not clear.

5. Conclusion

Single reactive cysteine variants of C*c*O in positions at both the N- and P-side were successfully constructed. Labeling of the CS-base variant and the cysteine variants of C*c*O with the pH indicator dye fluorescein shows that unique labeling positions were introduced into the enzyme. Neither the mutations in the CS base variant nor the additional introduction of single cysteine residues at the sites selected here affect the function of the enzyme. Similarly, the modification with fluorescein at the N-side of C*c*O did not interfere with the function of C*c*O. Thus, the described cysteine variants are well suited as labeling sites for further studies investigating the mechanism of proton pumping in C*c*O. First spectroscopic analysis using the bound pH indicator dye fluorescein revealed a negative surface charge of the cytoplasmic surface of CcO in detergent micelles, indicating that the C*c*O surface contributes to the negative charge at the N-side of the membrane. In addition, the buffer capacity at the cytoplasmic C*c*O surface is very high, higher than at the surface of the proton pump bacteriorhodopsin. The polarity of the environment at the cytoplasmic C*c*O surface depends on the redox state of the enzyme and it is higher in the oxidized state.

Acknowledgements

This work was supported by Deutsche Forschungsgemeinschaft Grants SFB 472 (to H. M.) and partially SFB 449 (to U. A.), the Max-Planck-Gesellschaft, and the Cluster of Excellence Frankfurt "Macro-molecular Complexes".

References

[1] J.R. Fetter, J. Qian, J. Shapleigh, J.W. Thomas, A. García-Horsman, E. Schmidt, J. Hosler, G.T. Babcock, R.B. Gennis, S. Ferguson-Miller, Possible proton relay pathways in cytochrome c oxidase, Proceedings of the National Academy of Sciences, 92 (1995) 1604-1608.

[2] J.A. Garcia-Horsman, A. Puustinen, R.B. Gennis, M. Wikstrom, Proton transfer in cytochrome bo3 ubiquinol oxidase of Escherichia coli: Second-site mutations in subunit I that restore proton pumping in the mutant Asp135.fwdarw.Asn, Biochemistry, 34 (1995) 4428-4433.

[3] S. Iwata, C. Ostermeier, B. Ludwig, H. Michel, Structure at 2.8 A resolution of cytochrome c oxidase from Paracoccus denitrificans, Nature, 376 (1995) 660-669.

[4] J. Koepke, E. Olkhova, H. Angerer, H. Muller, G. Peng, H. Michel, High resolution crystal structure of Paracoccus denitrificans cytochrome c oxidase: new insights into the active site and the proton transfer pathways, Biochimica et biophysica acta, 1787 (2009) 635-645.

[5] J.W. Thomas, A. Puustinen, J.O. Alben, R.B. Gennis, M. Wikstrom, Substitution of asparagine for aspartate-135 in subunit I of the cytochrome bo ubiquinol oxidase of Escherichia coli eliminates proton-pumping activity, Biochemistry, 32 (1993) 10923-10928.

[6] P. Brzezinski, P. Ädelroth, Pathways of Proton Transfer in Cytochrome c Oxidase, Journal of Bioenergetics and Biomembranes, 30 (1998) 99-107.

[7] E. Forte, F.M. Scandurra, O.-M.H. Richter, E. D'Itri, P. Sarti, M. Brunori, B. Ludwig, A. Giuffrè, Proton Uptake upon Anaerobic Reduction of the Paracoccus denitrificans Cytochrome c Oxidase: A Kinetic Investigation of the K354M and D124N Mutants†, Biochemistry, 43 (2004) 2957-2963.

[8] A.A. Konstantinov, S. Siletsky, D. Mitchell, A. Kaulen, R.B. Gennis, The roles of the two proton input channels in cytochrome c oxidase from Rhodobacter sphaeroides probed by the effects of site-directed mutations on time-resolved electrogenic intraprotein proton transfer, Proceedings of the National Academy of Sciences, 94 (1997) 9085-9090.

[9] H. Michel, J. Behr, A. Harrenga, A. Kannt, CYTOCHROME C OXIDASE: Structure and Spectroscopy, Annual Review of Biophysics and Biomolecular Structure, 27 (1998) 329-356.

[10] I. Belevich, D.A. Bloch, N. Belevich, M. Wikstrom, M.I. Verkhovsky, Exploring the proton pump mechanism of cytochrome c oxidase in real time, Proceedings of the National Academy of Sciences of the United States of America, 104 (2007) 2685-2690.

[11] D.M. Popovic, A.A. Stuchebrukhov, Proton pumping mechanism and catalytic cycle of cytochrome c oxidase: Coulomb pump model with kinetic gating, FEBS letters, 566 (2004) 126-130.

[12] P. Rich, Towards an Understanding of the Chemistry of Oxygen Reduction, Functional Plant Biology, 22 (1995) 479-486.

[13] L. Qin, J. Liu, D.A. Mills, D.A. Proshlyakov, C. Hiser, S. Ferguson-Miller, Redox-dependent conformational changes in cytochrome C oxidase suggest a gating mechanism for proton uptake, Biochemistry, 48 (2009) 5121-5130.

[14] P. Brzezinski, R.B. Gennis, Cytochrome c oxidase: exciting progress and remaining mysteries, J Bioenerg Biomembr, 40 (2008) 521-531.

[15] L. Salomonsson, K. Faxen, P. Adelroth, P. Brzezinski, The timing of proton migration in membrane-reconstituted cytochrome c oxidase, Proceedings of the National Academy of Sciences of the United States of America, 102 (2005) 17624-17629.

[16] S. Yoshikawa, K. Muramoto, K. Shinzawa-Itoh, Proton-pumping mechanism of cytochrome C oxidase, Annual review of biophysics, 40 (2011) 205-223.

[17] L.S. Busenlehner, L. Salomonsson, P. Brzezinski, R.N. Armstrong, Mapping protein dynamics in catalytic intermediates of the redox-driven proton pump cytochrome c oxidase,

Proceedings of the National Academy of Sciences of the United States of America, 103 (2006) 15398-15403.
[18] K. Kirchberg, H. Michel, U. Alexiev, Net Proton Uptake Is Preceded by Multiple Proton Transfer Steps upon Electron Injection into Cytochrome c Oxidase, Journal of Biological Chemistry, 287 (2012) 8187-8193.
[19] P. Brzezinski, P. Adelroth, Proton-controlled electron transfer in cytochrome c oxidase: functional role of the pathways through Glu 286 and Lys 362, Acta Physiol Scand Suppl, 643 (1998) 7-16.
[20] M. Karpefors, P. Adelroth, A. Aagaard, H. Sigurdson, M. Svensson Ek, P. Brzezinski, Electron-proton interactions in terminal oxidases, Biochimica et biophysica acta, 10 (1998) 1-2.
[21] D.A. Mills, S. Ferguson-Miller, Proton uptake and release in cytochrome c oxidase: separate pathways in time and space?, Biochimica et biophysica acta, 1365 (1998) 46-52.
[22] S. Papa, N. Capitanio, G. Villani, G. Capitanio, A. Bizzoca, L.L. Palese, V. Carlino, E. De Nitto, Cooperative coupling and role of heme a in the proton pump of heme-copper oxidases, Biochimie, 80 (1998) 821-836.
[23] H. Michel, Bioenergetics: Proton pumping by cytochrome c oxidase, Nature, 402 (1999) 602-603.
[24] B.C. Hill, Intermediate forms of cytochrome oxidase observed in transient kinetic experiments and those visited in the catalytic cycle, Biochimica et biophysica acta, 1655 (2004) 256-262.
[25] J.P. Hosler, S. Ferguson-Miller, D.A. Mills, Energy Transduction: Proton Transfer Through the Respiratory Complexes, Annual Review of Biochemistry, 75 (2006) 165-187.
[26] S. Papa, G. Capitanio, P. Luca Martino, Concerted involvement of cooperative proton-electron linkage and water production in the proton pump of cytochrome c oxidase, Biochimica et biophysica acta, 1757 (2006) 1133-1143.
[27] M.I. Verkhovsky, I. Belevich, D.A. Bloch, M. Wikstrom, Elementary steps of proton translocation in the catalytic cycle of cytochrome oxidase, Biochimica et biophysica acta, 1757 (2006) 401-407.
[28] S.A. Siletsky, A.A. Konstantinov, Cytochrome c oxidase: charge translocation coupled to single-electron partial steps of the catalytic cycle, Biochimica et biophysica acta, 1817 (2012) 476-488.
[29] D. Zaslavsky, R.C. Sadoski, S. Rajagukguk, L. Geren, F. Millett, B. Durham, R.B. Gennis, Direct measurement of proton release by cytochrome c oxidase in solution during the F→O transition, Proceedings of the National Academy of Sciences of the United States of America, 101 (2004) 10544-10547.
[30] K. Faxen, L. Salomonsson, P. Adelroth, P. Brzezinski, Inhibition of proton pumping by zinc ions during specific reaction steps in cytochrome c oxidase, Biochimica et biophysica acta, 1757 (2006) 388-394.
[31] A. Namslauer, A.S. Pawate, R.B. Gennis, P. Brzezinski, Redox-coupled proton translocation in biological systems: proton shuttling in cytochrome c oxidase, Proceedings of the National Academy of Sciences of the United States of America, 100 (2003) 15543-15547.
[32] P. Adelroth, M.S. Ek, D.M. Mitchell, R.B. Gennis, P. Brzezinski, Glutamate 286 in cytochrome aa3 from Rhodobacter sphaeroides is involved in proton uptake during the reaction of the fully-reduced enzyme with dioxygen, Biochemistry, 36 (1997) 13824-13829.
[33] S. Hallen, T. Nilsson, Proton transfer during the reaction between fully reduced cytochrome c oxidase and dioxygen: pH and deuterium isotope effects, Biochemistry, 31 (1992) 11853-11859.
[34] U. Alexiev, R. Mollaaghababa, H.G. Khorana, M.P. Heyn, Evidence for long range allosteric interactions between the extracellular and cytoplasmic parts of bacteriorhodopsin

from the mutant R82A and its second site revertant R82A/G231C, The Journal of biological chemistry, 275 (2000) 13431-13440.
[35] U. Alexiev, I. Rimke, T. Pohlmann, Elucidation of the nature of the conformational changes of the EF-interhelical loop in bacteriorhodopsin and of the helix VIII on the cytoplasmic surface of bovine rhodopsin: a time-resolved fluorescence depolarization study, Journal of molecular biology, 328 (2003) 705-719.
[36] U. Alexiev, P. Scherrer, T. Marti, H.G. Khorana, M.P. Heyn, Time-resolved surface charge change on the cytoplasmic side of bacteriorhodopsin, FEBS letters, 373 (1995) 81-84.
[37] K. Heyne, J. Herbst, B. Dominguez-Herradon, U. Alexiev, R. Diller, Reaction Control in Bacteriorhodopsin: Impact of Arg82 and Asp85 on the Fast Retinal Isomerization, Studied in the Second Site Revertant Arg82Ala/Gly231Cys and Various Purple and Blue Forms of Bacteriorhodopsin, The Journal of Physical Chemistry B, 104 (2000) 6053-6058.
[38] M. Gutman, E. Nachliel, The dynamic aspects of proton transfer processes, Biochimica et Biophysica Acta (BBA) - Bioenergetics, 1015 (1990) 391-414.
[39] Y. Marantz, E. Nachliel, A. Aagaard, P. Brzezinski, M. Gutman, The proton collecting function of the inner surface of cytochrome c oxidase from Rhodobacter sphaeroides, Proceedings of the National Academy of Sciences, 95 (1998) 8590-8595.
[40] A. Shinobu, G.J. Palm, A.J. Schierbeek, N. Agmon, Visualizing proton antenna in a high-resolution green fluorescent protein structure, Journal of the American Chemical Society, 132 (2010) 11093-11102.
[41] U. Alexiev, R. Mollaaghababa, P. Scherrer, H.G. Khorana, M.P. Heyn, Rapid long-range proton diffusion along the surface of the purple membrane and delayed proton transfer into the bulk, Proceedings of the National Academy of Sciences of the United States of America, 92 (1995) 372-376.
[42] M. Sajadi, Y. Ajaj, I. Ioffe, H. Weingartner, N.P. Ernsting, Terahertz absorption spectroscopy of a liquid using a polarity probe: a case study of trehalose/water mixtures, Angewandte Chemie (International ed. in English), 49 (2010) 454-457.
[43] U. Alexiev, T. Marti, M.P. Heyn, H.G. Khorana, P. Scherrer, Covalently bound pH-indicator dyes at selected extracellular or cytoplasmic sites in bacteriorhodopsin. 2. Rotational orientation of helices D and E and kinetic correlation between M formation and proton release in bacteriorhodopsin micelles, Biochemistry, 33 (1994) 13693-13699.
[44] P. Scherrer, U. Alexiev, T. Marti, H.G. Khorana, M.P. Heyn, Covalently bound pH-indicator dyes at selected extracellular or cytoplasmic sites in bacteriorhodopsin. 1. Proton migration along the surface of bacteriorhodopsin micelles and its delayed transfer from surface to bulk, Biochemistry, 33 (1994) 13684-13692.
[45] C. Ostermeier, A. Harrenga, U. Ermler, H. Michel, Structure at 2.7 A resolution of the Paracoccus denitrificans two-subunit cytochrome c oxidase complexed with an antibody FV fragment, Proceedings of the National Academy of Sciences of the United States of America, 94 (1997) 10547-10553.
[46] C. Yanisch-Perron, J. Vieira, J. Messing, Improved M13 phage cloning vectors and host strains: nucleotide sequences of the M13mp18 and pUC19 vectors, Gene, 33 (1985) 103-119.
[47] B. Ludwig, Cytochrome c oxidase from Paracoccus denitrificans, Methods in enzymology, 126 (1986) 153-159.
[48] G. Kleymann, C. Ostermeier, B. Ludwig, A. Skerra, H. Michel, Engineered Fv fragments as a tool for the one-step purification of integral multisubunit membrane protein complexes, Bio/technology (Nature Publishing Company), 13 (1995) 155-160.
[49] H. Witt, V. Zickermann, B. Ludwig, Site-directed mutagenesis of cytochrome c oxidase reveals two acidic residues involved in the binding of cytochrome c, Biochimica et biophysica acta, 1230 (1995) 74-76.

[50] U. Alexiev, T. Marti, M.P. Heyn, H.G. Khorana, P. Scherrer, Surface charge of bacteriorhodopsin detected with covalently bound pH indicators at selected extracellular and cytoplasmic sites, Biochemistry, 33 (1994) 298-306.
[51] Y. Koutalos, T.G. Ebrey, H.R. Gilson, B. Honig, Octopus photoreceptor membranes. Surface charge density and pK of the Schiff base of the pigments, Biophysical journal, 58 (1990) 493-501.
[52] W. Junge, S. McLaughlin, The role of fixed and mobile buffers in the kinetics of proton movement, Biochimica et biophysica acta, 890 (1987) 1-5.
[53] L. Ojemyr, T. Sanden, J. Widengren, P. Brzezinski, Lateral proton transfer between the membrane and a membrane protein, Biochemistry, 48 (2009) 2173-2179.
[54] P. Adelroth, P. Brzezinski, Surface-mediated proton-transfer reactions in membrane-bound proteins, Biochimica et biophysica acta, 12 (2004) 1-3.
[55] W. Humphrey, A. Dalke, K. Schulten, VMD: visual molecular dynamics, J Mol Graph, 14 (1996) 33-38, 27-38.

Figure Legends

Fig. 1. (A) Overall architecture of the two core subunits of C*c*O embedded in a lipid bilayer. Subunit I is shown in *green*, subunit II in *cyan*. Cu_A, Cu_B, heme *a*, heme a_3 and the residues D124 and K354 are indicated. B) D- and K-proton pathways (pdb: 3HB3). The figure was prepared with VMD [55].

Fig. 2. Position of amino acids in C*c*O exchanged to cysteine. (A) Side view. Light grey: subunit I, dark grey: subunit II. The arrows indicate the two proton uptake pathways to the hemes starting at D124 (*red*, "D-pathway") and at K354 (*orange*, "K-pathway"), respectively and possible proton exit pathways (*blue*). (B) and (C) View from the cytoplasmic side. Acidic amino acids are colored in *red* and *histidines* in blue. (B) Amino acids exchanged to cysteine at the entrance of the D-pathway are marked in *green*, D124 is indicated in *cyan*. (C) Amino acids exchanged to cysteine at the entrance of the K-pathway are marked in *green*, K354 is indicated in *cyan*.

Fig. 3. Absorption spectra of single-reactive cysteine variants (*red*) in comparison to wild type (*black*). Comparison of the absorption spectra from the „cysteine-less" base variant CS (*red*-oxidized, *cyan*-reduced) and wild type (*black dotted*). Inset: Reduction of cytochrome *c* by CS and wild type monitored by 550 nm. The calculated turnover number is 500 s^{-1}. Conditions: 10 mM potassium phosphate buffer pH 7.4, 40 mM KCl, 1 mM EDTA, 0.05% LM, RT.

Fig. 4. (A) Absorption spectra of CS-P302C unlabeled (dashed line) and labeled (solid line) with IAF. The arrow marks the pH-sensitive absorption band of fluorescein. Conditions: 10 mM potassium phosphate buffer pH 9.0, 50 mM KCl und 0.05 % LM. (B) 12 % SDS-PAGE of the 2-subunit variant CS-I302C-AF (Lane 2) and CS (Lane 3). Lane 1: Molecular weight marker (MW), Sizes in kD. (C) Comparison of the absorption spectra of CS-K299C-AF in the oxidized (black dotted line) and reduced (black line) state.

Fig. 5. (A) Absorption spectra of fluorescein at different pH-values. (B) Absorption spectra of the labeled variant CS-I302C-AF at pH 9 (solid line). For comparison the absorbance of the unlabeled protein is shown (dashed). (C) Absorption spectrum of wild type C*c*O at different pH-values. Between 485 and 505 nm the absorption spectra of C*c*O are not pH dependent. The arrow marks the pH-sensitive absorption band of fluorescein. Conditions as in Fig. 4.

Fig. 6. (A) pH titration data and fit curves according to the Henderson-Hasselbalch equation for C*c*O-bound fluorescein in position 302 on the N-side at the entrance of the K-pathway at 10 mM, 100 mM and 150 mM KCl. (B) Gouy-Chapman-Plot for CS-I302-AF. The surface charge density is plotted against the salt concentration.

Fig. 7. (A) Difference spectra of oxidized minus reduced enzyme. (B) Fluorescein difference spectra (labeled minus unlabeled protein) in the oxidized (*solid*) and reduced (*dashed*) state of CS-T26C-AF. (C) The wavelengths of the absorption maxima of cystein-bound amido fluorescein (C-AF) in 150 mM KCl and in water/ethanol-mixture at pH 9 plotted against the dielectric constants. (D) Close up of amino acids in C*c*O exchanged to cysteine at the entrance of the D-pathway. Grey: protein, red: amino acids exchanged to cysteine, cyan: water molecules. The wavelength of the absorption maximum (λ_{max}) of the cysteine bound fluoresein in the oxidized state at pH 9, as well as the λ_{max} shift upon reduction of the solubilized enzyme are determined. (E) Close up of amino acids in C*c*O exchanged to cysteine at the entrance of the K-pathway. Grey: protein, yellow: amino acids exchanged to cysteine, cyan: water molecules. The wavelength of the absorption maximum (λ_{max}) of the cysteine bound fluorescein in the oxidized state at pH 9, as well as the λ_{max} shift upon reduction of the solubilized enzyme are determined. The λ_{max}-shift values are the mean from 2-3 independent measurements. SEM is given.

Tables

Table 1: Turn over number (TON) of the different cysteine variants and wild type.

Variant	TON (s^{-1})	Variant	TON (s^{-1})	Variant	TON (s^{-1})
CS-T26C	497±20	CS-S295C	490±20	CS-H^{II}29C	489±20
CS-N27C	502±20	CS-K299C	504±20	CS-D^{II}30C	521±20
CS-P123C	513±20	CS-P301C	507±20	CS-R^{II}130C	511±20
CS-P128C	495±20	CS-I302C	499±20	wild type	512±20

Table 2: Label stoichiometry for the binding of IAF to the CS base and the CS-„single"-cysteine variants (in %).

Sample	C*c*O/AF (%)	Sample	C*c*O/AF (%)	Sample	C*c*O/AF (%)
CS-T26C-AF	40	CS-S295C-AF	46	CS-H^{II}29C-AF	0
CS-N27C-AF	0	CS-K299C-AF	26	CS-D^{II}30C-AF	0
CS-P123C-AF	25	CS-P301C-AF	75	CS-R^{II}130C-AF	0
CS-P128C-AF	55	CS-P302C-AF	92	CS	0

Table 3: The buffer capacity quotient $\Delta A/\Delta c_{H+}$ of the AF-labeled cysteine variants, as well as of wild type C*c*O - LM micelles, LM detergent micelles and bacteriorhodopsin- LM micelles with soluble fluorescein. SD is given.

Sample	**$\Delta A/\Delta c_{H+}$ (mOD/µM)**
CS-T26C-AF	0.18±0.06
CS-P123C-AF	0.11±0.07
CS-P128C-AF	0.25±0.09
CS-S295C-AF	0.27±0.05
CS-K299C-AF	0.13±0.07
CS-P301C-AF	0.16±0.07
CS-I302C-AF	0.11±0.05
C*c*O (0.05 % LM) + 25 µM Flu	1.1±0.5
0.05 % LM + 25 µM Flu	3.7±0.9
Bacteriorhodopsin (0.05 % LM) + 25 µM Flu	3.7±0.5

Figures

Figure 1

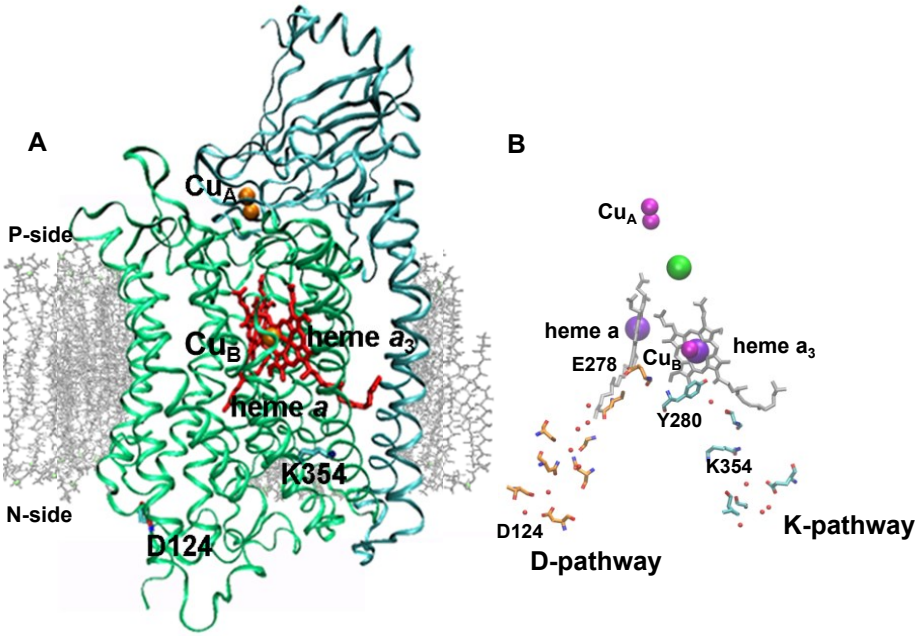

Figure 2

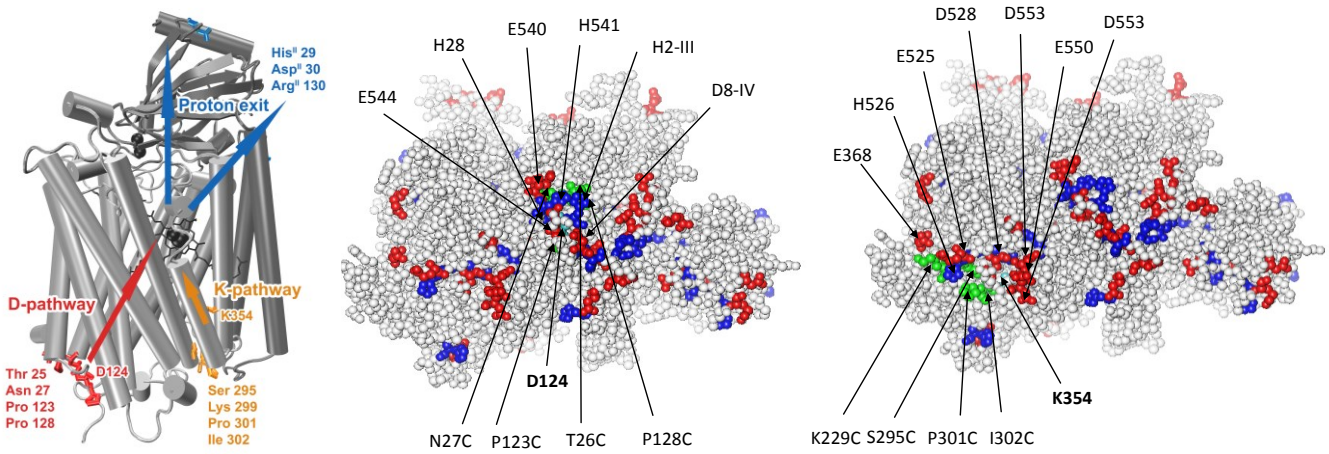
His[II] 29
Asp[II] 30
Arg[II] 130
Proton exit
D-pathway
K-pathway
K354
D124
Thr 25
Asn 27
Pro 123
Pro 128
Ser 295
Lys 299
Pro 301
Ile 302
H28
E540
H541
H2-III
E544
D8-IV
D124
N27C
P123C
T26C
P128C
D528
D553
D553
E525
E550
H526
E368
K354
K229C
S295C
P301C
I302C

Figure 3

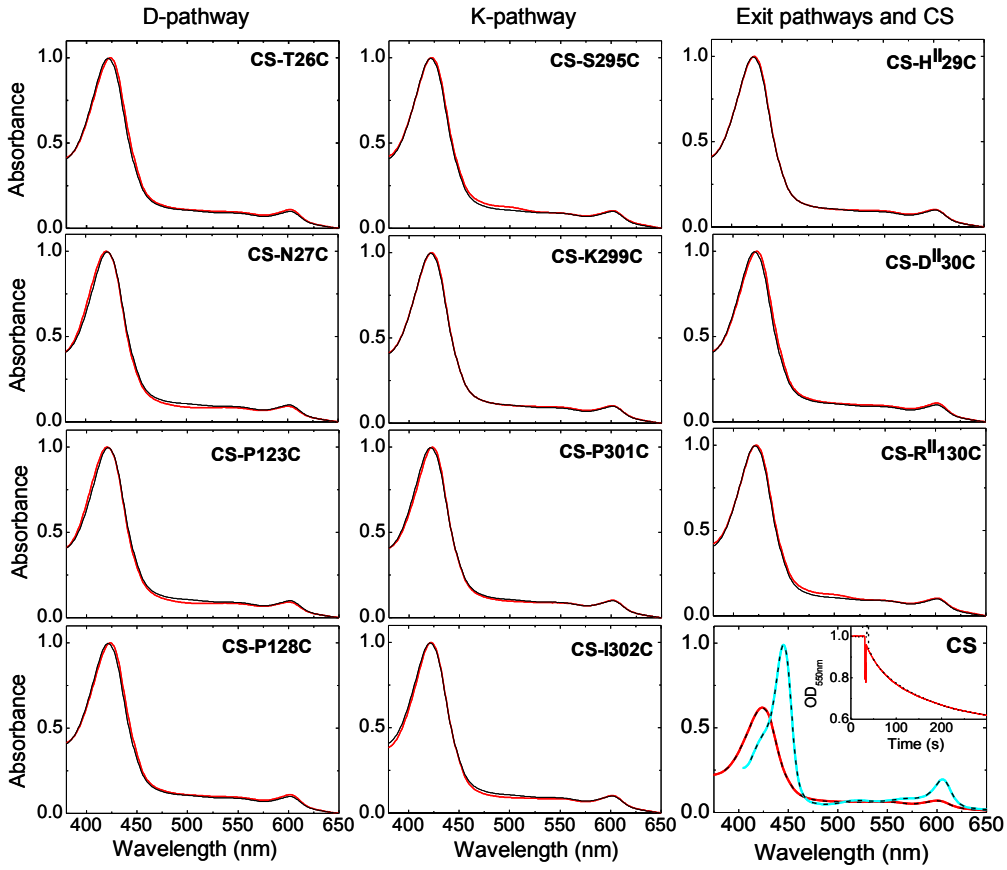
D-pathway
K-pathway
Exit pathways and CS
CS-T26C
CS-S295C
CS-H^{II}29C
CS-N27C
CS-K299C
CS-D^{II}30C
CS-P123C
CS-P301C
CS-R^{II}130C
CS-P128C
CS-I302C
CS
Absorbance
Wavelength (nm)
OD$_{550nm}$
Time (s)

Figure 4

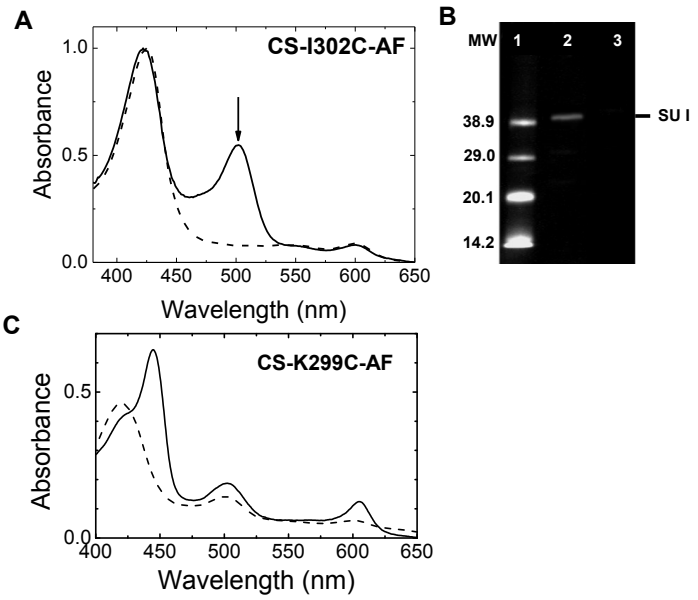
A
CS-I302C-AF
Absorbance
1.0
0.5
0.0
400
450
500
550
600
650
Wavelength (nm)
B
MW
1
2
3
38.9
29.0
20.1
14.2
SU I
C
CS-K299C-AF
Absorbance
0.5
0.0
400
450
500
550
600
650
Wavelength (nm)

Figure 5

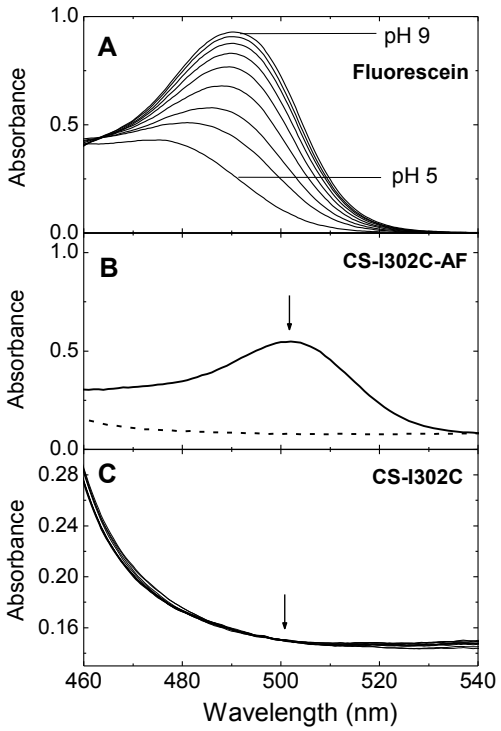
A
pH 9
Fluorescein
pH 5
B
CS-I302C-AF
C
CS-I302C
Absorbance
Wavelength (nm)
1.0
0.5
0.0
0.28
0.24
0.20
0.16
460
480
500
520
540

Figure 6

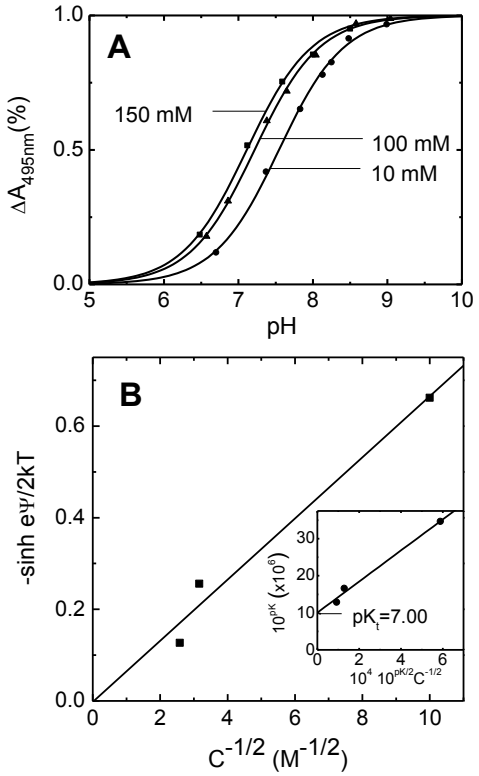
A
150 mM
100 mM
10 mM
ΔA495nm(%)
pH
B
-sinh eΨ/2kT
C-1/2 (M-1/2)
10pK (x10^6)
pKt=7.00
10^4 10^pK/2 C^-1/2

Figure 7

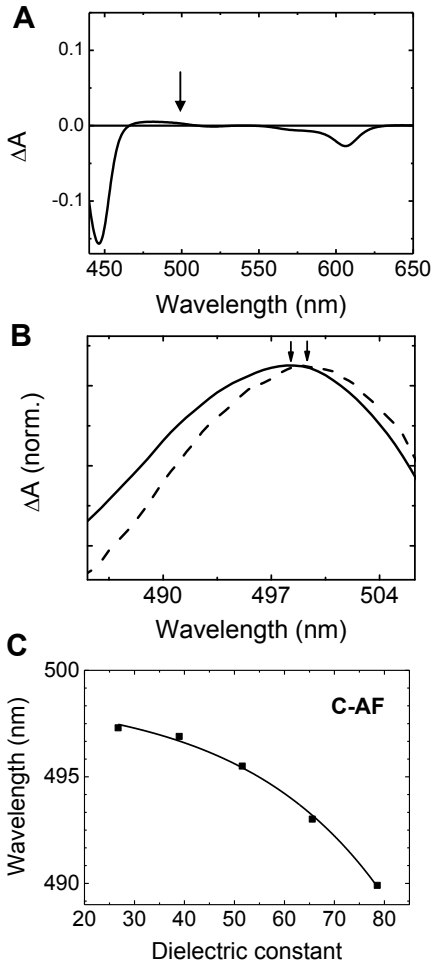

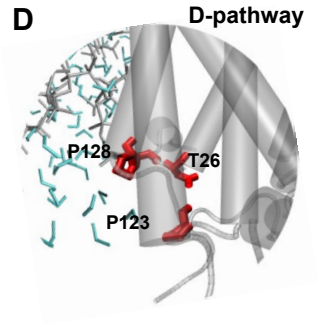

Position	λ_{max} (oxid.) (nm)	$\Delta\lambda$ (nm) upon reduction
26	498.3±0.1	+(1.1±0.2)
123	497.3±0.8	+(2.2±1.1)
128	498.3±0.6	+(2.1±0.9)

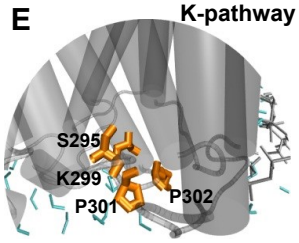

Position	λ_{max}(oxid.) (nm)	$\Delta\lambda$ (nm) upon reduction
295	502.5±0.3	n.d.
299	501.2±0.3	+(0.8±0.6)
301	496.6±0.4	+(2.2±0.5)
302	502.2±0.3	n.d.